On AC electrokinetics in the regime of high voltage and high ion diffusivity ratio

By A. Balaji, S. Mirjalili AND A. Mani

1. Motivation and objectives

Systems in which aqueous electrolytes interact with the electric fields induced by charged surfaces are encountered in electrochemical applications involving chemical separation, sample preconcentration, or reactions in microfluidic devices. Previous work has examined cases in which binary-symmetric or binary-asymmetric electrolytes interact with ion-selective membranes or electrodes in the presence of DC or AC applied voltages. The aim of this study is to extend this type of analysis to examine potential hydrodynamic instabilities in plasma systems.

In studies involving ion-selective membranes and DC applied voltages, the phenomena of concentration polarization and subsequent formation of extended space charge (ESC) regions in the fluid have been shown to cause electroconvective instability, whereby an ordered (at lower voltages) or chaotic (at higher voltages) flow develops in the fluid and enhances the transport of ions (Rubinstein & Zaltzman 2000; Druzgalski *et al.* 2013). Persistent electroconvection is not seen in systems with inert (blocking) electrodes under DC applied voltage, but the application of a high enough AC voltage in the appropriate frequency range has been suggested to lead to formation of transient ESC regions (Olesen *et al.* 2010). Kim *et al.* (2019) numerically studied such AC systems with blocking electrodes in the context of the coupled Poisson-Nernst-Planck and Stokes equations and showed that the formation of such ESC regions permits growth of electroconvective instability and development of a chaotic flow. This phenomenon was observed in systems with binary-symmetric electrolytes and binary-asymmetric electrolytes, in which one ion has higher mass diffusivity than the other.

Typically, previous studies were performed at relatively modest voltages ($O(100\mathrm{V_T})$) (thermal volts) and ion diffusivity ratios ($O(10)$ at most), since higher voltages and diffusivity ratios are not encountered in electrochemical applications with aqueous electrolytes (Olesen *et al.* 2010; Kim *et al.* 2019; Amrei *et al.* 2019). However, the phenomenon of plasma dielectric barrier discharge (DBD) typically occurs at much higher applied voltages. Furthermore, the cations and ions present in a plasma have mass diffusivities that differ from one another by several orders of magnitude. As a first step toward modeling of DBD systems, we study the simplest set of equations that contains the basic physics of nonthermal plasma discharges—conservation equations for the charged species, and Poisson's equation to determine the electric field (Georghiou *et al.* 2005). Through numerical simulation, we aim to study whether electroconvection can occur in plasma regimes, and if so, whether strong mixing effects would occur as a result. Several physical phenomena have been neglected in these equations, but our results contribute to a qualitative understanding of behavioral trends in electrokinetic systems in the plasma regime. Furthermore, our results motivate and guide subsequent study of plasma discharges using the fluid model and incorporating effects that are neglected here (coupling to hydrodynamics, reactions, thermal non-equilibrium, etc.).

The range of voltages and diffusivity ratios studied is approaching the regime of DBD, in which voltages of $O(10^5 \mathrm{V_T})$ and diffusivity ratios of $O(10^4)$ are seen. Selection of an appropriate range of frequencies for AC simulations requires the identification of a characteristic timescale over which the system evolves, as has been done by Kim *et al.* (2019). As shown by Bazant *et al.* (2004), the behavior of the two-electrode, symmetric-ion system is shown to have a characteristic timescale $\tau_{\mathrm{RC}} = \lambda_D L/(2D_{\mathrm{eff}})$, where D_{eff} is simply taken to be the diffusivity of either ion, since both ions have the same diffusivity in the classical problem. Here, λ_D is the Debye length, which describes the thickness of highly charged thin zones called electric double layers (EDLs) that form near charged surfaces, and L is the length scale of the domain. Kim *et al.* (2019) suggest that in the case of asymmetric ions, the value of D_{eff} should be taken as the arithmetic mean of the two ion diffusivities in the problem: $(D^+ + D^-)/2$.

Rigorous identification of the system timescale has not been performed for the high voltages and diffusivity ratios that are of interest in this work. Therefore, a model problem similar to that used by Bazant *et al.* (2004) is studied first. The first part of this study examines the dynamics when a DC voltage is applied and the system relaxes to a steady solution. Identification of the timescale, historically called τ_{RC}, for this process in the regime of high voltages and diffusivity ratios allows for a selection of appropriate frequencies that will be used in the AC simulations. The second part of this study examines the dynamics when AC voltages are applied. Specifically, we are interested in the development of ESC regions that are necessary for the eventual occurrence of chaotic electroconvection in 2D simulations that we intend to perform in a later work.

2. Governing equations

We are ultimately interested in studying DBD plasma, a non-thermal plasma generated at atmospheric pressures under sinusoidal applied voltage. In non-thermal plasmas, cations and neutral gas atoms remain near room temperature while the anions (electrons) alone have a much higher temperature. Use of a fluid model is appropriate for plasmas at atmospheric pressure, in which relaxation to a Boltzmann distribution occurs very quickly compared to macroscopic changes in the system. (i.e., frequency of applied voltage and charge dynamics) (Wu & Kunhardt 1988; Kogelschatz 2003; Georghiou *et al.* 2005; Corke *et al.* 2010). Therefore, we consider conservation equations for positive and negative ions, in addition to Poisson's equation for the electric field. The drift-diffusion approximation is used to model the fluxes of ions, as is commonly done in numerical simulations of such phenomena (Georghiou *et al.* 2005).

For plasmas at atmospheric pressures, cations and neutrals are in thermal equilibrium with each other. In non-thermal plasmas, heating on the order of only a few degrees Kelvin is expected for the neutral and cationic species (Georghiou *et al.* 2005; Corke *et al.* 2010). The effect of these temperature variations on transport properties is neglected, in order to consider the simplest set of equations that demonstrates the physics of incipient electroconvection. Thermal variations in the electron temperature are also neglected. As such, mass diffusivity of the anions and cations, D^- and D^+, respectively, are assumed to be constant in time and space within this study.

Realistically, ionization, attachment, electron–positive ion recombination, negative ion–positive ion recombination, and photo-ionization are expected to occur in plasma DBD devices (Georghiou *et al.* 2005). At atmospheric pressure, the formation of discharges through ionization avalanches occurs over the nanosecond timescale, and free radical

reactions occur on scales varying between microseconds and milliseconds (Kogelschatz 2003). These timescales are short (or, in the worst case, on the same order) compared to the macroscopic system timescales. A more accurate simulation should incorporate free radical reactions, particularly at higher applied frequencies. However, as a starting point, we neglect all reaction terms in the species conservation equations. As such, we are studying a model problem in which a fixed number of ions in a domain is allowed to evolve in response to a time-varying electric field.

Electroconvection is only seen in 2D and 3D geometries, in which the Navier-Stokes equations governing the hydrodynamic effects are coupled to the transport equations for the ions. However, the charge dynamics that are precursors to electroconvection can be observed and studied in one dimension much more inexpensively than in two. 1D ESC regions that extend into the bulk of the domain are necessary for the formation of electroconvective instability and subsequent multi-dimensional flow. Cases without these charged regions cannot exhibit classical electroconvection. We do not purport to study electroconvection itself in our study. However, we do examine the 1D features that must be present in order for electroconvection to form, and we identify regions in the parameter space in which these structures are or are not observed. The neutral gas is assumed to be incompressible, which yields $u = 0$ in the 1D geometry between two inert electrodes. We further assume that the plasma is weakly ionized and non-magnetized.

We are interested in a binary ionic system with equal valences, ± 1, for anions and cations. Note, however, that while the cations (gaseous ions) and anions (electrons) have the same valence, their mass diffusivities differ significantly. Steric and Stern-layer effects are not considered in this work. Such effects are expected to be considerable at high voltages (Kilic *et al.* 2007; Olesen *et al.* 2010; Gillespie 2015), but we defer a more comprehensive study including such effects to later work.

Using the assumptions listed above, one can simplify the species conservation equations into the Nernst-Planck equations. If we denote the electric potential with ϕ and the concentration of the positive and negative ions with c^+ and c^-, respectively, then in dimensional form we have

$$\frac{\partial c^{\pm}}{\partial t} = \nabla \cdot (D^{\pm} \nabla c^{\pm}) \pm \nabla \cdot (D^{\pm} \frac{1}{\mathrm{V_T}} c^{\pm} \nabla \phi), \tag{2.1}$$

where $\mathrm{V_T} = k_B T/(ze)$ is the thermal volt, k_B is the Boltzmann constant ($1.38 \times 10^{-23} J/K$), T is the temperature of cations and neutrals (constant, in this work), and e is the elementary charge ($1.6 \times 10^{-19} C$). The electric potential is coupled to the concentration fields via Gauss's law,

$$\nabla^2 \phi = -\frac{ze(c^+ - c^-)}{\varepsilon}, \tag{2.2}$$

where ε is the electrical permittivity of the gas. We use appropriate reference quantities to non-dimensionalize Eqs. (2.1)-(2.2). The length of the 1D domain, L, is used to non-dimensionalize length scales. The anion diffusivity is the reference diffusivity, and the anion diffusion timescale, L^2/D^-, is used for time. Initial ion (anion or cation) concentration, c_0, is used for concentrations, and the thermal volt, $\mathrm{V_T}$ is used for electric potential.

In plasma DBD, $D^+ \ll D^-$. The smaller diffusivity, which represents the gaseous ions and background gas as opposed to electrons, should be used as a reference diffusivity when considering hydrodynamic effects. However, we choose to study the case of $D^+ \gg D^-$, as was studied by Kim *et al.* (2019). Conclusions regarding the dynamics of this system

are still generalizable. Identical features are seen in the case of $D^+ \ll D^-$; these features have opposite-signed charge and are geometrically reflected.

With this nondimensionalization, four dimensionless parameters are used to characterize the problem in the chosen 1D setting: (1) the dimensionless EDL thickness given by $\epsilon = \lambda_D/L$, where $\lambda_D = \sqrt{\varepsilon k_B T/(2c_0(ze)^2)}$, (2) the ionic diffusivity ratio given by $\hat{D} = D^+/D^-$, (3) the dimensionless maximum applied AC voltage, $\hat{V} = V_{\max}/\mathrm{V_T}$, and (4) the dimensionless applied AC frequency denoted by $\hat{\omega}$. Note that a multi-dimensional study coupled to the momentum transport equation would introduce other parameters that are not discussed here.

In dimensionless form, Eq. (2.1) for the positive and negative ions and Eq. (2.2) for the electric potential are given by

$$\frac{\partial \hat{c}^+}{\partial \hat{t}} = \hat{D}\nabla \cdot (\nabla \hat{c}^+ + \hat{c}^+ \nabla \hat{\phi}), \tag{2.3}$$

$$\frac{\partial \hat{c}^-}{\partial \hat{t}} = \nabla \cdot (\nabla \hat{c}^- - \hat{c}^- \nabla \hat{\phi}), \tag{2.4}$$

$$-2\epsilon^2 \nabla^2 \hat{\phi} = \hat{c}^+ - \hat{c}^-, \tag{2.5}$$

respectively, where dimensionless variables carry a hat symbol. The electrodes are assumed to be ideally polarizable with zero Faradaic current. Hence, for both electrodes, the boundary conditions for the charged species are no flux of either ion, giving

$$(\nabla \hat{c}^{\pm} \pm \hat{c}^{\pm} \nabla \hat{\phi})_{\hat{x}=0,1} = 0, \tag{2.6}$$

in dimensionless form. For the electric potential, we have Dirichlet time-varying boundary conditions. We keep the left electrode at $\hat{x} = 0$ at a fixed voltage of 0,

$$\hat{\phi}_{\hat{x}=0} = 0, \tag{2.7}$$

while varying the voltage on the other electrode with dimensionless frequency of $\hat{\omega}$,

$$\hat{\phi}_{\hat{x}=1} = \hat{V}\cos(\hat{\omega}\hat{t}). \tag{2.8}$$

A special case of Eq. (2.8) is $\hat{\omega} = 0$, corresponding to a DC voltage applied at time $\hat{t} = 0$, similar to the study by Bazant *et al.* (2004).

3. Numerical methods

We solve the dimensionless Eqs. (2.3)-(2.8) via a finite-volume approach similar to that of Kim *et al.* (2019). A staggered grid is employed with concentration and electric field values stored on cell centers and fluxes stored on cell edges. A stretched mesh with a higher concentration of mesh points at the walls is used to resolve the EDLs. Second-order central differences are used for spatial discretization, with special attention to maintain exact conservation for Eqs. (2.3)-(2.4) at the discrete level. To achieve conservation, we align the left edge of the first cell with the left electrode surface and the right edge of the last cell with the right electrode. Fluxes of both ions at these edges are set exactly to zero, as required by Eq. (2.6). The Dirichlet boundary conditions for electric potential given by Eqs. (2.7)-(2.8) are incorporated into the discrete version of Gauss's law, Eq. (2.5). For the first and last edge, we use one-sided differences to compute $\nabla\hat{\phi}$. For temporal discretization, we use a second-order implicit Euler scheme in δ-form (entailing linearization of nonlinear terms) with three iterations per time step. This allows for use

of a time step (Δt) longer than the shortest timescales in the problem, which are prohibitively short and rapidly decaying. Finally, in order to reduce the bandwidth of the large sparse linear system solved for each iteration, we follow Druzgalski *et al.* (2013) by reordering variables in the vector of unknowns containing $\hat{c}^{\pm}$ and $\hat{\phi}$.

4. Results

In order to identify a characteristic timescale, τ_{RC}, for the system and investigate its dependence on $\hat{V}$ and $\hat{D}$, simulations of the DC case are performed first. In these cases, $\hat{\omega} = 0$ while $\hat{V}$ and $\hat{D}$ are varied by several orders of magnitude. The characteristic timescale is shown to exhibit dependence on $\hat{V}$ and $\hat{D}$. Furthermore, the size of thin structures that appear in the simulations is also shown to exhibit dependence on $\hat{V}$ and $\hat{D}$.

Next, we perform AC simulations in which $\hat{V}$, $\hat{D}$, and $\hat{\omega}$ are varied over several orders of magnitude. The goal of these simulations is to determine the cases for which a breaking of symmetry and transition to 2D electroconvective chaos is possible, based on the charge dynamics observed in the respective 1D simulations. These simulations reveal four distinct regimes of behavior, in which the charge dynamics of the system evolve in distinct patterns. Three of these behaviors are seen in the unity diffusivity ratio case in addition to non-unity diffusivity ratio cases, while one behavior is seen exclusively for non-unity diffusivity ratios. Two of these behaviors contain ESC regions that are necessary for electroconvective instability to develop. Regions in the $\hat{\omega}$-$\hat{V}$ parameter space in which each behavior is observed are identified for different diffusivity ratios.

4.1. *DC simulations*

In the DC simulations, the domain is initialized with a uniform concentration of cations and anions: $c^{+}(x,0) = c^{-}(x,0) = 1$. Selecting $\hat{\phi}(x,0) = \hat{V}x$ and $\hat{\omega} = 0$ represents the application of constant voltage across the electrodes starting at time $\hat{t} = 0$. Simulations are performed with $\hat{V} = \{625, 1250, 2500, 5000, 10, 000\}$ and $\hat{D} = \{1, 10^1, 10^2, 10^3, 10^4\}$.

An instantaneous image of the concentration profiles is shown in Figure 1 for the case of $\hat{V} = 10,000$ and $\hat{D} = 10^4$, at $\hat{t} = 7.425 \times 10^{-5}$. Figure 1(a) shows the entire profile, while Figure 1(b,c) shows zoomed-in images of the left and right electrode, respectively, highlighting the EDLs that form next to the electrodes. Note that a thin interface is observed in the middle of the domain. This type of interface, at which electromigration and diffusion fluxes are competing with each other at a highly localized zone far from the electrodes, seems to be a unique feature that appears when high voltages are applied to a pair of blocking electrodes.

On the right side of the interface, the ion with larger diffusivity is depleted, while the ion with smaller diffusivity takes on a small but finite value. Classically, this is identified as an ESC region. On the left side of the interface, we find $O(1)$ salt concentration and electroneutrality. Though this work is concerned with gaseous ions, the term salt is used to indicate the presence of both cations and anions together, as has been done in classical studies of aqueous electrolytes. Starting from a location close to the right EDL, the interface separating these two regions moves across the domain (from right to left when $\hat{D} > 1$ and $\partial\hat{\phi}/\partial x > 0$) over time. Meanwhile, the interface also changes in thickness as it moves. Once the interface reaches the left EDL, the system quickly reaches a state of charge depletion everywhere except in the EDL zones. Very little change occurs

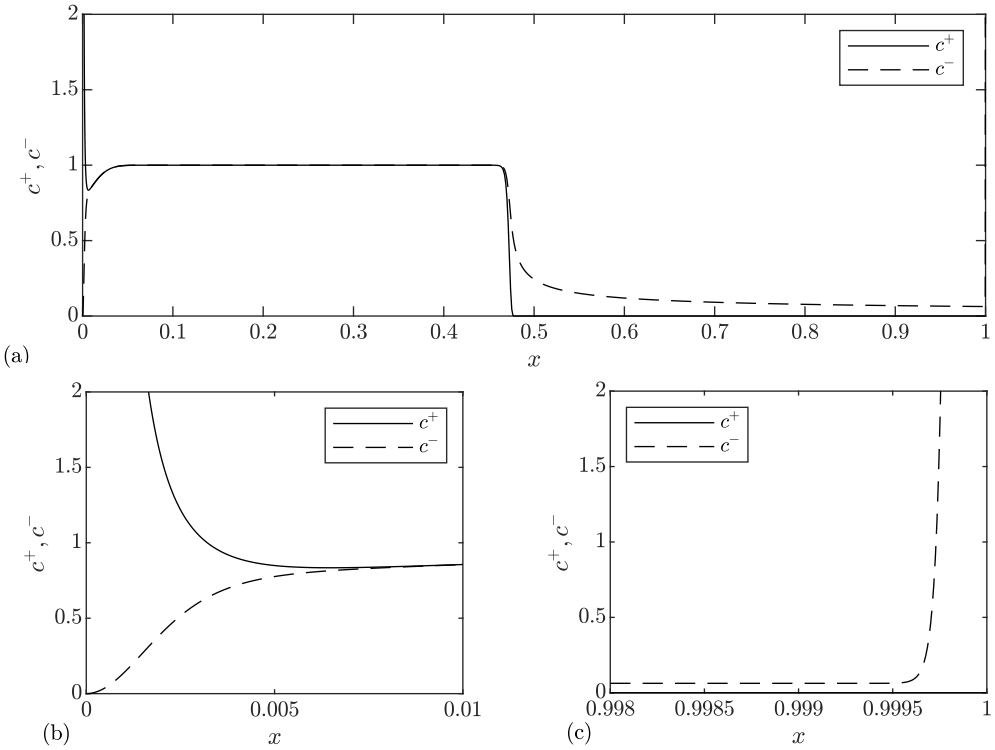

FIGURE 1. Profiles of concentration fields for the case of $\hat{V} = 10,000$ and $\hat{D} = 10^4$, at $\hat{t} = 7.425 \times 10^{-5}$. The entire profile is shown in (a), while a close-up of the left electrode (at which $\hat{\phi} = 0$) is shown in (b) and a close-up of the right electrode (at which $\hat{\phi} = \hat{V}$) is shown in (c).

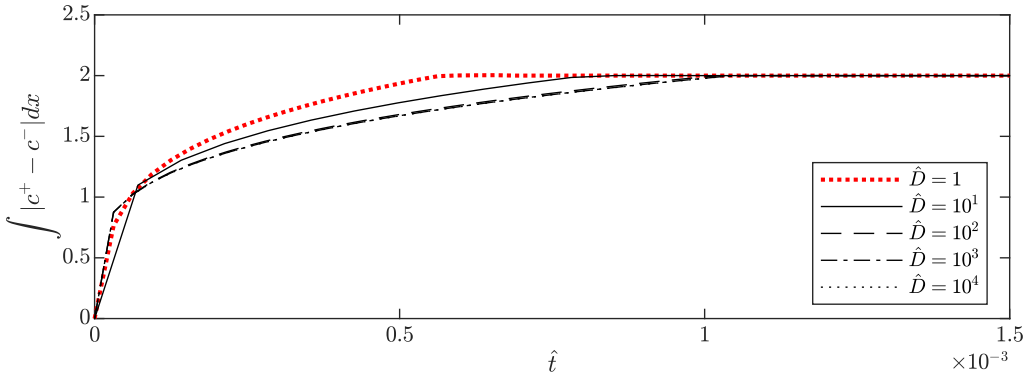

FIGURE 2. Amount of charge in the domain (integrated charge density) as a function of time for five different values of $\hat{D}$, with $\hat{V} = 10,000$. Curves for $\hat{D} = 10^2$, $\hat{D} = 10^3$, and $\hat{D} = 10^4$ are shown on top of one another.

once this state is reached, so the characteristic timescale for this system should reflect the amount of time required for the system to reach this final state.

The suggestion offered by Kim *et al.* (2019) to use the arithmetic mean $D_{\text{eff}} = 1/(2(D^+ + D^-))$ in τ_{RC} would imply that $\tau_{\text{RC}} = \epsilon/(2D_{\text{eff}}) \to \epsilon/D^+$ as $\hat{D} \to \infty$. There-

fore, the timescale of the system's relaxation should scale inversely with D^+. However, our results indicate that this is not the case for the high-voltage, high-diffusivity-ratio regime. The amount of charge in the domain (integrated charge density) is shown as a function of time in Figure 2 for five different values of $\hat{D}$. For each curve, the amount of charge in the domain starts at 0 due to the initial condition. As the interface moves and the ESC region grows, the amount of charge in the domain increases. This occurs until the interface reaches the left EDL, and the amount of charge in the domain reaches a value of 2, indicating that the all the ions in the domain have accumulated in their respective EDLs, near the electrodes. In this state, the rest of the domain is depleted of ions.

Comparing the curves shown in Figure 2 reveals that the time at which the depleted state is reached is not affected significantly by changes in $\hat{D}$ over several orders of magnitude once $\hat{D}$ is made large enough. This suggests that a different choice of D_{eff} is required. The harmonic mean, $D_{\text{eff}} = 2D^+D^-/(D^+ + D^-)$, which appears in the salt transport equation, is a choice consistent with the results shown here. As $\hat{D} \to \infty$, $D_{\text{eff}} \to 2D^-$, thereby implying that $\tau_{\text{RC}} = \epsilon/2D_{\text{eff}} \to \epsilon/(4D^-)$. When D^- is held fixed, the timescale no longer depends on $\hat{D}$ once $\hat{D}$ is made large enough, as is seen in Figure 2. Physically, this suggests that the process of overall salt diffusion plays a crucial role in the dynamics of the system at very high voltage and diffusivity ratio. This behavior is approached asymptotically as $\hat{D}$ is made sufficiently large.

A more detailed analysis of the dynamics is performed by examining the velocity at which the interface moves, u_δ. It is expected that the timescale should depend on the velocity through the relation $\tau_{\text{RC}} \sim 1/u_\delta$. In cases with $\hat{D} = 1$, two of these interfaces are formed in the high-voltage regime. One moves from right to left, while the other moves from left to right. Termination occurs in the center of the domain, where the two interfaces meet each other. In the proceeding analyses, the right-side interface (which moves from right to left) is used for obtaining the results for $\hat{D} = 1$ cases. Additionally, the presence of two interfaces moving toward each other with velocity u_δ suggests that each interface would only need to move across half the domain in order to reach the depleted state for the symmetric case.

The right and left edges of the interface are identified at each time step based on the degree to which electromigration and diffusion fluxes are in balance locally. The position of the interface is taken to be the mean of the left and right edges, and a velocity is determined using a first-order finite difference. The velocity of the interface, u_δ is shown as a function of time for $\hat{V} = 10,000$ in Figure 3(a). Note that the velocity is negative since the interface is moving from right to left for the cases studied. As exemplified in Figure 3(a), the interface velocities exhibit an asymptotic behavior with increasing $\hat{D}$. This phenomenon is observed for all choices of $\hat{V}$ studied, further supporting the choice of harmonic mean as the correct effective diffusivity in the high-voltage and high-diffusivity-ratio regime. Note that the non-unity $\hat{D}$ cases lie almost on top of one another, demonstrating that asymptotic behavior is reached very quickly as $\hat{D}$ is increased.

In the classical limit, dependence of τ_{RC} on $\hat{V}$ is not expected. However, examination of results at fixed $\hat{D}$ and varying $\hat{V}$ reveals that this is not the case in the high-voltage regime. The velocity of the interface is shown as a function of time for $\hat{D} = 10^4$ in Figure 3(b). The plots for other values of $\hat{D}$ are very similar to this representative example. For all cases, these curves collapse when u_δ is scaled by $\hat{V}^{1/2}$, as shown. Based on this, we determine that the speed of the interface scales as $u_\delta \sim \hat{V}^{1/2}$. Furthermore, we expect the characteristic timescale to exhibit the dependence $\tau_{\text{RC}} \sim 1/u_\delta \sim \hat{V}^{-1/2}$.

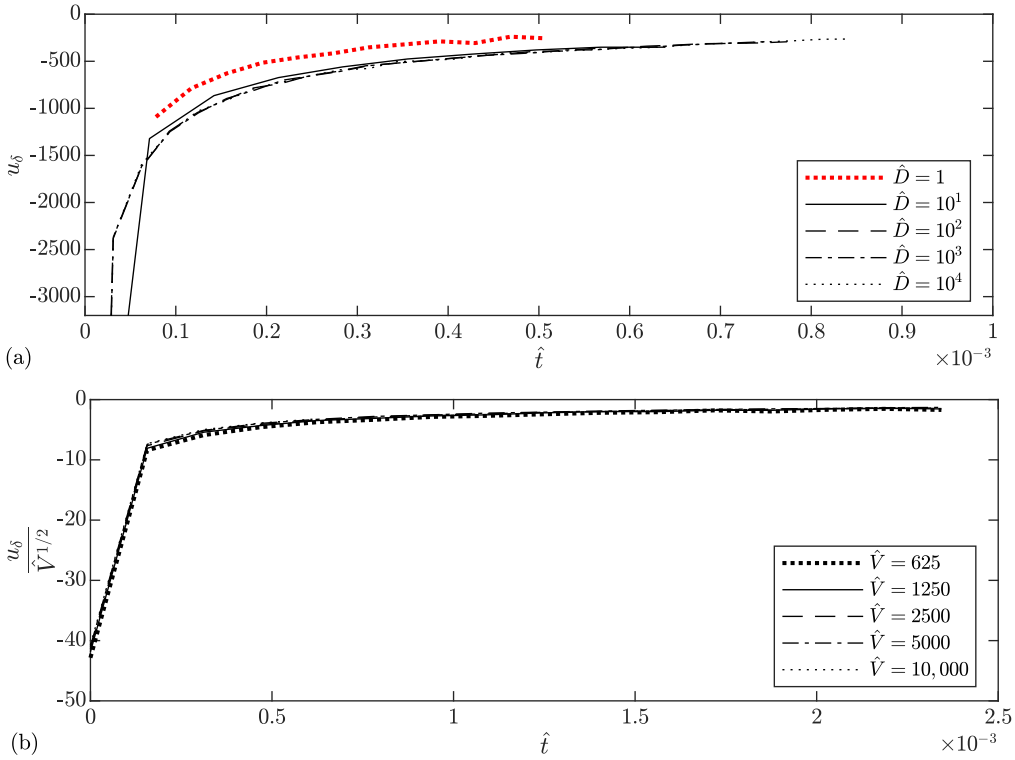

FIGURE 3. Interface velocity (u_δ) as a function of time. In (a), $\hat{V} = 10,000$ and diffusivity ratio is varied. In (b), $\hat{D} = 10,000$ and applied voltage is varied. In (b), u_δ is scaled by $\hat{V}^{1/2}$, demonstrating collapse.

The thickness of the interface, δ, and its dependence on $\hat{V}$ and $\hat{D}$ partially determine the spatial resolution required in simulations. δ is plotted as a function of time for $\hat{V} = 10,000$ (with varying diffusivity ratio) in Figure 4(a) and for $\hat{D} = 10^4$ (with varying voltage) in Figure 4(b). Figure 4(a) shows that higher diffusivity ratios are responsible for thicker interfaces. As demonstrated previously, an asymptotic behavior is observed at higher diffusivity ratios. Accordingly, the curves for $\hat{D} = 10^3$ and $\hat{D} = 10^4$ are very close to each other. In contrast, the dependence of δ on $\hat{V}$ is much stronger, as seen in Figure 4(b). Scaling by $\hat{V}^{-1/4}$ leads to a collapse of the data as shown. Therefore, in the high-voltage and high-diffusivity-ratio regime, $\delta \sim \hat{V}^{-1/4}$. Thinner features are expected when the voltage is increased. This behavior and the collapse when scaled by $\hat{V}^{-1/4}$ are seen for all values of $\hat{D}$ studied.

4.2. *AC simulations*

In the AC simulations, the domain is initialized with a uniform concentration of cations and anions: $c^+(x,0) = c^-(x,0) = 1$. The initial condition for potential is selected to be $\hat{\phi}(x,0) = \hat{V}x$. Simulations are performed with $\hat{V} = \{625, 1250, 2500, 5000, 10,000\}$ and $\hat{D} = \{1, 10^2, 10^4\}$. Additional simulations with $\hat{V} = \{40, 75, 110, 145, 180\}$ are performed for $\hat{D} = 1$, in order to allow comparison with values obtained by Kim *et al.* (2019).

Values of $\hat{\omega}$ are selected on the basis of information about the timescale revealed in the DC simulations. Specifically, the harmonic mean, $D_{\text{eff}} = 2D^+D^-/(D^+ + D^-)$, is

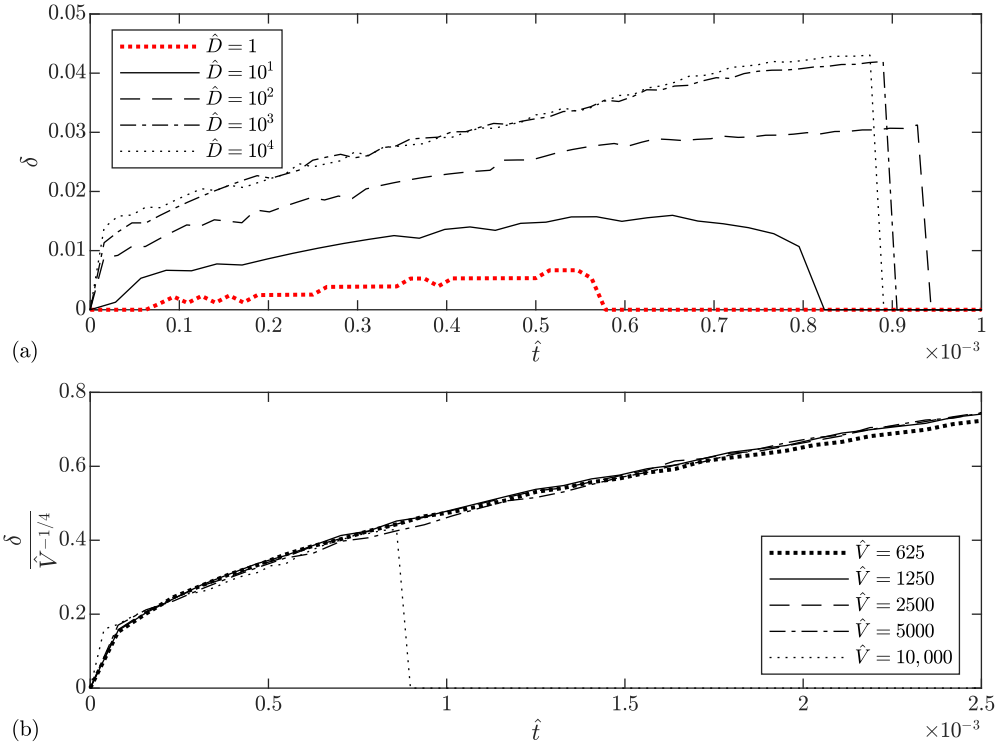

FIGURE 4. Interface thickness, δ, as a function of time (t). In (a), $\hat{V} = 10,000$ and $\hat{D}$ is varied, while in (b), $\hat{D} = 10^4$ and $\hat{V}$ is varied. In (b), δ is scaled by $\hat{V}^{-1/4}$, demonstrating collapse.

an appropriate effective diffusivity that can be inserted into the RC timescale, $\tau_{\mathrm{RC}} = \epsilon/(2D_{\mathrm{eff}})$. Based on this, we introduce a reduced frequency,

$$\widetilde{\omega} = \hat{\omega}\tau_{\mathrm{RC}} = \hat{\omega}\frac{\epsilon}{4(D^+D^-)/(D^+ + D^-)}. \tag{4.1}$$

Simulations are performed for $\widetilde{\omega} = \{0.04, 0.2, 1, 5\}$ at $\hat{D} = 10^2$ and $\hat{D} = 10^4$. For $\hat{D} = 1$, additional frequencies of $\widetilde{\omega} = \{0.008, 25\}$ are tested as well. Each simulation is run for at least five periods of oscillation or five RC timescales, whichever is larger. The behavior becomes periodic after transients elapse, so the last two periods of each simulation are assessed in order to determine the type of behavior observed for a given $\hat{D}$, $\hat{V}$, and $\hat{\omega}$.

Regimes of behavior for the case of the unity diffusivity ratio are displayed for the low-voltage region in Figure 5(a), along with points from the study of Kim *et al.* (2019). Instantaneous representative concentration profiles for the three regimes identified in these simulations are depicted in Figure 5(b-d).

Starting at the upper left corner of Figure 5(a), the initial type of behavior seen at sufficiently low frequencies and sufficiently high voltages is similar to the result achieved in DC simulations. This behavior is termed depletion behavior, since there is enough time for depletion to occur over most of the domain. The ions in the domain have enough time to be transported entirely into the EDLs near either electrode before the oscillating voltage changes signs. This depleted state is shown in Figure 5(b). The EDL at the left

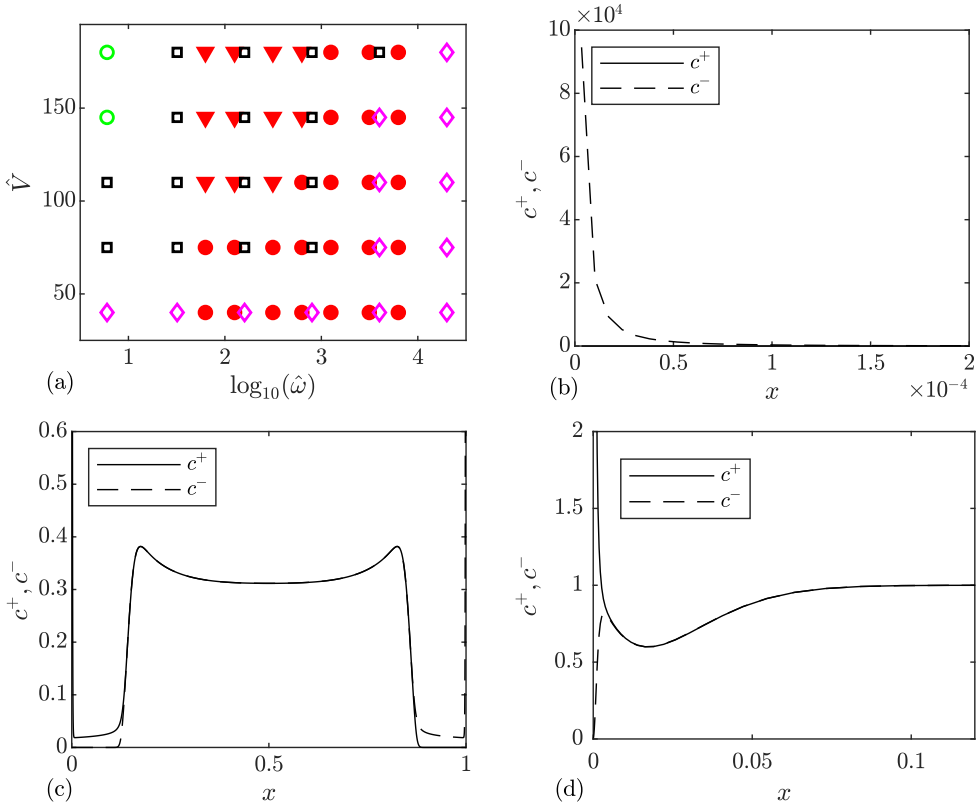

FIGURE 5. (a) Regime diagram in the $\hat{V}$ versus $\hat{\omega}$ space, for $\hat{D} = 1$. Unfilled symbols correspond to findings from this work, while solid symbols represent results from the work of Kim *et al.* (2019). For results of this work: ◯ represents depletion behavior, □ represents ESC-with--steady-bulk behavior, and ◊ represents no-ESC behavior. For the results of Kim *et al.* (2019): ▼ represents chaotic cases, and ● represents non-chaotic cases. Instantaneous representative snapshots of (b) depletion behavior, (c) ESC-with-steady-bulk behavior, and (d) no-ESC behavior are also depicted.

electrode is shown here, along with a small part of the depleted bulk. Another EDL exists at the other electrode, but with opposite sign. The bulk is depleted of ions of either sign.

As the applied voltage changes signs for cases that exhibit depletion behavior, the ions contained in either EDL will be transported toward the other opposite electrode, where they will form a new EDL. The ions are given sufficient time for this transport to occur completely, again leading to a depleted state throughout the bulk. In other words, the timescale of oscillation is relatively slow compared to the timescale of this ionic transport process. The depleted state is present for the vast majority of each period, signifying that this regime is not conducive to chaotic behavior in the 2D case.

As voltage is decreased or frequency is increased, a new type of behavior is observed in which ESC regions are formed and there is not enough time for depletion to occur. This behavior is termed ESC-with-steady-bulk behavior, and an instantaneous representative snapshot of the concentration profiles is shown in Figure 5(c). In this state, two ESC regions are found on either side of a non-depleted and electroneutral central bulk region. The presence of salt in the bulk region persists as the voltage oscillates, and ESCs form on either side of it in a periodic fashion. The sign of charge in each ESC oscillates as the

voltage oscillates. The non-depleted bulk region acts as a reservoir for either ESC. Thus, unlike the depletion behavior cases, this prevents the two ESC regions from meeting in the center of the domain and the subsequent depletion of salt from the bulk. This regime is conducive to hydrodynamic chaos in the 2D case, because of the presence of ESC regions that could grow unstable.

As voltage is decreased or frequency is increased even further, another behavior is observed in which ESC zones are not formed, hence the term no-ESC regime. This type of behavior, depicted in Figure 5(d), is often seen in classical studies performed at very low voltages. Because the timescale of the oscillation is very short compared to that of electromigration, EDLs are not strongly charged and a majority of the domain is electroneutral. Depicted in Figure 5(d) is a region near the left electrode which shows an EDL immediately adjacent to the electroneutral bulk. A similar structure with opposite charge is seen at the other electrode. This case is not conducive to chaos in 2D simulations because of the absence of ESC regions that could become unstable. Therefore, $\hat{\omega}$ is shown to have a non-monotonic effect on likelihood of a 2D simulation to become chaotic.

A comparison to existing 2D simulations in the low-voltage region is presented in Figure 5(a). Kim *et al.* (2019) classify simulations as chaotic or non-chaotic by comparing the maximum induced velocity and the electroviscous velocity scale. Comparison of these results with the behavioral regimes discovered in this work reveals qualitative agreement. This is expected, since 2D simulations are expected to remain 1D until an ESC is formed and electroconvective instability is given time to grow. Though electroconvection can only be seen in 2D or 3D geometries, the formation of an ESC is a 1D phenomenon. Kim *et al.* (2019) explored the region at which 1D concentration profiles transition between ESC-with-steady-bulk behavior and no-ESC behavior, but they did not explore the lower limit of $\hat{\omega}$, at which depletion behavior occurs.

A regime diagram for unity diffusivity ratio and all voltages is depicted in Figure 6(a). The lower section of the plot is the same data presented in Figure 5(a), while the upper portion presents data for the high-voltage region, which is explored later in this work for non-unity diffusivity ratios. For high voltages, only two regimes are observed when $\hat{D} = 1$: depletion behavior and ESC-with-steady-bulk behavior. Intuitively, no-ESC behavior is expected if frequency is made large enough. The boundary between ESC-with-steady-bulk and no-ESC behavior is oriented such that even higher frequencies are required to achieve no-ESC behavior when voltage is increased. Similarly, the transition from depletion behavior to ESC-with-steady-bulk behavior occurs at higher frequencies for higher voltages.

Regime diagrams for the $\hat{D} = 10^2$ and $\hat{D} = 10^4$ cases are shown in Figure 6(b,c). Note that the depletion behavior is also observed for the non-unity diffusivity ratio at high voltages and low frequencies. Additionally, the ESC-with-steady-bulk behavior is also seen at low voltages and high frequencies. This type of behavior occurs slightly differently in the non-unity diffusivity ratio cases, in comparison to the unity diffusivity ratio case. In both cases, the center of the domain contains a non-depleted and electroneutral region that persists throughout the simulation as the voltage oscillates. For the unity diffusivity ratio, one ESC forms on either side of this non-depleted zone. For non-unity diffusivity ratios, a single ESC forms on one side of the non-depleted zone for half of the oscillation period, and a single ESC forms on the other side of the non-depleted zone for the other half of the oscillation period. For both cases of ESC-with-steady-bulk behavior, the presence of this non-depleted zone prevents the ESC from growing and occupying

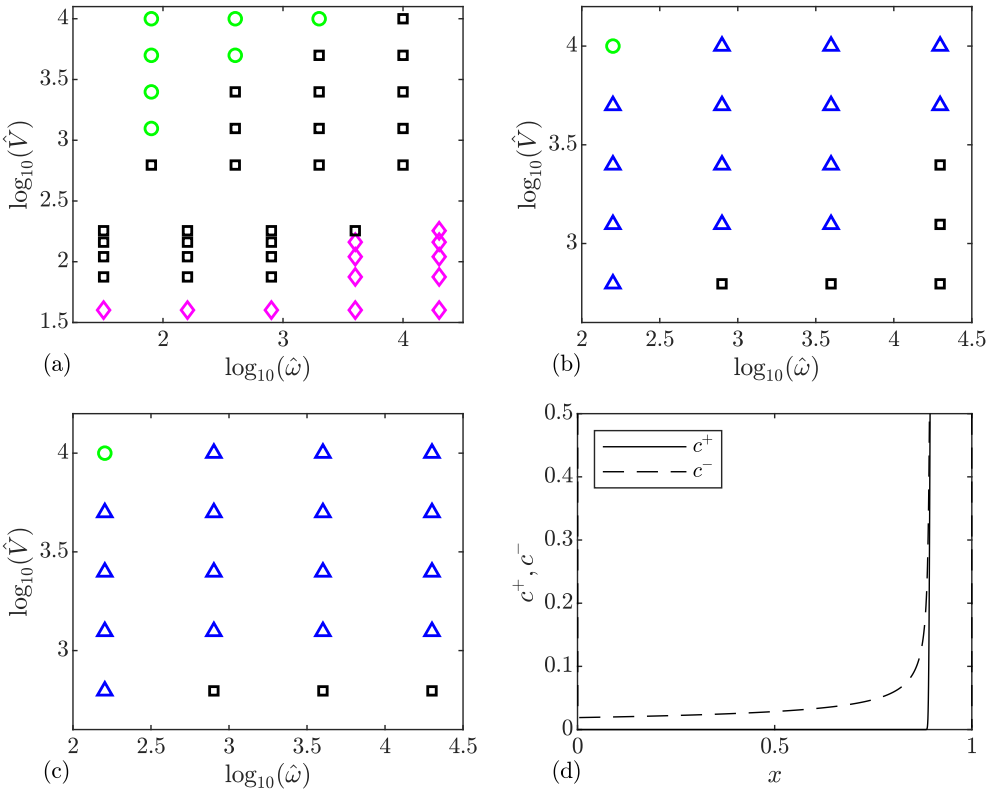

FIGURE 6. Regime diagrams in the $\hat{V}$ versus $\hat{\omega}$ space, for (a) $\hat{D} = 1$, (b) $\hat{D} = 10^2$, and (c) $\hat{D} = 10^4$. Each symbol corresponds to one of four behaviors identified: ◯ represents depletion behavior, □ represents ESC-with-steady-bulk behavior and △ and ◊ represents no-ESC behavior. An instantaneous representative snapshot of the asymmetric-ESC behavior is displayed in (d).

the majority of the domain. Ultimately, the presence of an ESC indicates that this case could grow unstable when simulated in 2D.

A new behavior is seen in Figure 6(b,c), termed the asymmetric-ESC behavior. This behavior appears between the depletion behavior and ESC-with-steady-bulk behavior regions, and it grows slightly more prominent as $\hat{D}$ is increased. An instantaneous representative snapshot of the concentration profiles for this behavior is shown in Figure 6(d). An ESC forms on one side of the domain, while an electroneutral zone forms on the other side. In some cases, the ESC occupies the majority of the domain, as depicted in Figure 6(d). This is generally observed at higher voltages and higher frequencies. At lower voltages and lower frequencies, the ESC occupies a smaller portion of the domain, while the electroneutral zone is more dominant. As noted before, the presence of an ESC in this case might lead to chaotic electroconvection in the 2D simulation. However, it cannot be determined from 1D data alone whether or not the larger-ESC cases are more likely than the smaller-ESC cases to become chaotic in 2D simulations.

5. Discussion and summary

In this study we performed 1D simulations of electrokinetic systems with asymmetric electrolytes between blocking electrodes under the application of high DC and AC voltages. We studied variations in applied voltage, applied frequency, and diffusivity ratio over several orders of magnitude.

In the DC simulations, we observed the presence of a moving interface that separated the ESC zone from the electroneutral part of the domain. For non-unity diffusivity ratios, this interface moved from one EDL to another, such that upon arrival at the destination, a vast majority of the domain would reach a salt-depleted state while the EDLs would each have a total charge of ± 1. The timescale of the system, which is connected to the velocity of this interface, was found to depend on the ionic diffusivity ratio and the applied voltage. Dependence on the diffusivity ratio was found to be governed by the harmonic mean, which is drastically different from the arithmetic mean in the limit of high diffusivity ratio. As such, at high diffusivity ratios, the timescale is essentially governed by the lower diffusivity instead of the higher one. The applied voltage had a stronger effect on the timescale of the system. Using $u_\delta \sim 1/\tau_c$, examination of the interface speed gave $\tau_{\mathrm{RC}} \sim \hat{V}^{-1/2}$. The interface thickness was found to also depend on both the diffusivity ratio and the applied voltage. Again, the interface thickness increased as the diffusivity ratio was increased, eventually reaching an asymptotic limit. Higher voltages resulted in thinner interfaces. Overall, from analysis of the timescales and interface thickness in these 1D DC simulations, we determined the appropriate range of frequencies and spatial resolution requirements for the AC simulations.

We then performed AC simulations, in which we observed four distinct regimes in the $\hat{D}$, $\hat{V}$, and $\hat{\omega}$ parameter space. These regimes were characterized by (1) depletion behavior, (2) ESC-with-steady-bulk behavior, (3) no-ESC behavior, and (4) asymmetric-ESC behavior. While the first three of these regimes were present for unity diffusivity ratio cases, the fourth region was seen to pervade the parameter space between the depleted and ESC-with-steady-bulk behaviors as the diffusivity ratios were increased. Overall, at a fixed high voltage and high diffusivity ratio, we observed a progression of behaviors from depletion behavior to asymmetric-ESC behavior, followed by ESC-with-steady-bulk behavior as $\hat{\omega}$ was increased. With regard to the propensity for electroconvective chaos, we noted that $\hat{\omega}$ has a non-monotonic effect.

It is important to point out that the 1D analyses presented here do not include the effects of the electric body forces on the momentum of the fluid. However, our study provides insight into the system dynamics primarily because of the tight connection between the instigation of electroconvective instabilities and the presence of ESC layers. In other words, we expect the cases exhibiting asymmetric-ESC and ESC-with-steady-bulk behavior to be most conducive to electroconvective instabilities and multi-dimensional chaotic flows. Conversely, cases exhibiting depletion behavior and no-ESC behavior are expected to remain 1D and non-chaotic. These predictions are in qualitative agreement with the 2D fully coupled simulations by Kim *et al.* (2019) at moderate voltages and low diffusivity ratios. Surely, 2D simulations which also solve the coupled Navier-Stokes equations would provide further insight into the chaotic behavior of electrokinetic systems at high voltages and high diffusivity ratios. Additionally, incorporation of effects specific to DBD plasmas, such as reactions and thermal non-equilibrium, would allow for quantitative analysis of such systems.

Acknowledgments

This investigation was funded by the Precourt Institute for Energy. A. Balaji is supported by the Charles H. Kruger Stanford Graduate Fellowship. The authors acknowledge use of computational resources from the Certainty cluster awarded by the National Science Foundation to CTR. Additionally, Dr. Mario Di Renzo is acknowledged for reviewing the work and providing helpful feedback.

REFERENCES

Amrei, S. H., Miller, G. H. & Ristenpart, W. D. 2019 Asymmetric rectified electric fields between parallel electrodes: Numerical and scaling analyses. *Phys. Rev. E* **99**, 062603.

Bazant, M. Z., Thornton, K. & Ajdari, A. 2004 Diffuse-charge dynamics in electrochemical systems. *Phys. Rev. E* **70**, 021506.

Corke, T. C., Enloe, C. L. & Wilkinson, S. P. 2010 Dielectric barrier discharge plasma actuators for flow control. *Annu. Rev. Fluid Mech.* **42**, 505–529.

Druzgalski, C., Andersen, M. & Mani, A. 2013 Direct numerical simulation of electroconvective instability and hydrodynamic chaos near an ion-selective surface. *Phys. Fluids* **25**, 110804.

Georghiou, G. E., Papadakis, A., Morrow, R. & Metaxas, A. 2005 Numerical modelling of atmospheric pressure gas discharges leading to plasma production. *J. Phys. D* **38**, R303.

Gillespie, D. 2015 A review of steric interactions of ions: Why some theories succeed and others fail to account for ion size. *Microfluid. Nanofluid.* **18**, 717–738.

Kilic, M. S., Bazant, M. Z. & Ajdari, A. 2007 Steric effects in the dynamics of electrolytes at large applied voltages. II. modified poisson-nernst-planck equations. *Phys. Rev. E* **75**, 021503.

Kim, J., Davidson, S. & Mani, A. 2019 Characterization of chaotic electroconvection near flat inert electrodes under oscillatory voltages. *Micromachines* **10**, 161.

Kogelschatz, U. 2003 Dielectric-barrier discharges: their history, discharge physics, and industrial applications. *Plasma Chem. Plasma P.* **23**, 1–46.

Olesen, L. H., Bazant, M. Z. & Bruus, H. 2010 Strongly nonlinear dynamics of electrolytes in large AC voltages. *Phys. Rev. E* **82**, 011501.

Rubinstein, I. & Zaltzman, B. 2000 Electro-osmotically induced convection at a permselective membrane. *Phys. Rev. E* **62**, 2238–2251.

Wu, C. & Kunhardt, E. E. 1988 Formation and propagation of streamers in N_2 and N_2-SF_6 mixtures. *Phys. Rev. A* **37**, 4396–4406.